Article

Not peer-reviewed version

Aspergilins A–B, Including a Unique Orsellinic Acid–Ribose–Pyridazinone-N-Oxide Hybrid, from the Mangrove Endophytic Fungus Aspergillus sp. A1E3

Binbin Wu , Chenglong Xu , Jianjun Chen * , Guangying Chen *

Posted Date: 26 October 2023

doi: 10.20944/preprints202310.1727.v1

Keywords: Aspergillus; pyridazinone-N□oxide hybrid; sterigmatocystin; antitumor; cell cycle arrest

Article

Aspergilins A–B, Including a Unique Orsellinic Acid–Ribose–Pyridazinone-N-Oxide Hybrid, from the Mangrove Endophytic Fungus *Aspergillus* sp. A1E3

Binbin Wu [1], Chenglong Xu [2] and Jianjun Chen [2,*], Guangying Chen [1,*]

[1] Key Laboratory of Tropical Medicinal Resource Chemistry of Ministry of Education, College of Chemistry and Chemical Engineering, Hainan Normal University, Haikou 571158, PR China; binbwu168@163.com (B.W.)
[2] School of Pharmaceutical Sciences, Guangdong Provincial Key Laboratory of New Drug Screening, Southern Medical University, 1838 Guangzhou Avenue North, Guangzhou 510515, PR China; xxuchenglong@163.com (C.X.)
* Correspondence: chgying123@163.com (G.C); jchen21@smu.edu.cn (J.C.) Tel.: (optional; include country code; if there are multiple corresponding authors, add author initials)

Abstract: Two new compounds, named aspergilins A (**1**) and B (**2**), were isolated from the mangrove endophytic fungus *Aspergillus* sp. A1E3 associated with the fruit of *Rhizophora mucronata*, together with averufanin (**3**). The planar structures and absolute configurations of these compounds were unambiguously established by extensive NMR investigations, quantum-chemical electronic circular dichroism (ECD) calculations, and single-crystal X-ray diffraction analysis. Most notably, the absolute configuration of aspergillin A (**1**) was determined by single-crystal X-ray diffraction analysis of its *tri*-pivaloyl derivative **4**, conducted with Cu Kα radiation, whereas that of averufanin (**3**) was first clarified by quantum-chemical ECD calculations. Aspergilin A is the first orsellinic acid–ribose–pyridazinone-*N*-oxide hybrid containing a unique β-oxo-2,3-dihydropyridazine 1-oxide moiety, whereas aspergilin B and averufanin are the sterigmatocystin and anthraquinone derivative, respectively. From the perspective of biosynthesis, aspergilin A could be originated from the combined assembly of three building blocks, viz., orsellinic acid, β-D-ribofuranose, and *L*-glutamine. It is an unprecedented alkaloid-*N*-oxide involving biosynthetic pathways of polyketide, pentose, and amino acid. Aspergilin B (**2**) exhibited potent antiproliferative activity against four cancer cell lines. In addition, Aspergilin B (**2**) dose-dependently induced G2/M phase arrest in HepG2 cells.

Keywords: *Aspergillus*; pyridazinone-*N*-oxide hybrid; sterigmatocystin; antitumor; cell cycle arrest

1. Introduction

Pyridazines and pyridazinones are rare in nature, but common building blocks for heterocyclic organic synthesis [1–4]. Maleic hydrazide, i.e., 1,2-dihydro-3,6-pyradizinedione, is a synthesized selective herbicides and temporary plant growth regulator commonly used to prevent sprouting of potato tubers, onions, garlic, and radishes, etc. during storage. It can also inhibit crop growth and extend the flowering period [5]. Pyridaben, another example of pyridazinones, is a broad-spectrum and contact killing acaricide. It is a mitochondrial electron transport inhibitor (METI) acaricide that promotes the formation of damaging oxygen and nitrogen radicals [6–8]. Pyridazine *N*-oxides are photoactivatable O(^{3}P) precursors for applications in organic synthesis and chemical biology [9], whereas pyridazinone *N*-oxides are relatively stable. To the best of our knowledge, all the pyridazinone *N*-oxides are synthetic compounds. To date, no natural products of pyridazinone *N*-oxides have been reported.

Mangrove endophytic fungi of the genus *Aspergillus* can produce structurally unique metabolites with diverse bioactivities [10–19]. In order to search for bioactive natural compounds with new structures, two new compounds, named aspergilins A (**1**) and B (**2**), were isolated from the mangrove endophytic fungus *Aspergillus* sp. A1E3 associated with the fruit of *Rhizophora mucronata*,

Preprints (www.preprints.org) | NOT PEER-REVIEWED | Posted: 26 October 2023 doi:10.20944/preprints202310.1727.v1

together with averufanin (**3**) [20–25] (Figure 1). To our knowledge, aspergilins A (**1**) is the first alkaloid-*N*-oxide featuring the presence of an unprecedented orsellinic acid–ribose–pyridazinone-*N*-oxide hybrid scaffold containing a unique β-oxo-2,3-dihydropyridazine 1-oxide moiety, whereas aspergilin B (**2**) and averufanin (**3**) are the sterigmatocystin and anthraquinone derivative, respectively. Herein, we report the isolation and structure identification of aspergilins A (**1**) and B (**2**), along with the absolute configuration clarification of averufanin (**3**). The antiproliferative activities of compounds **1**–**3** were also evaluated against four cancer cell lines.

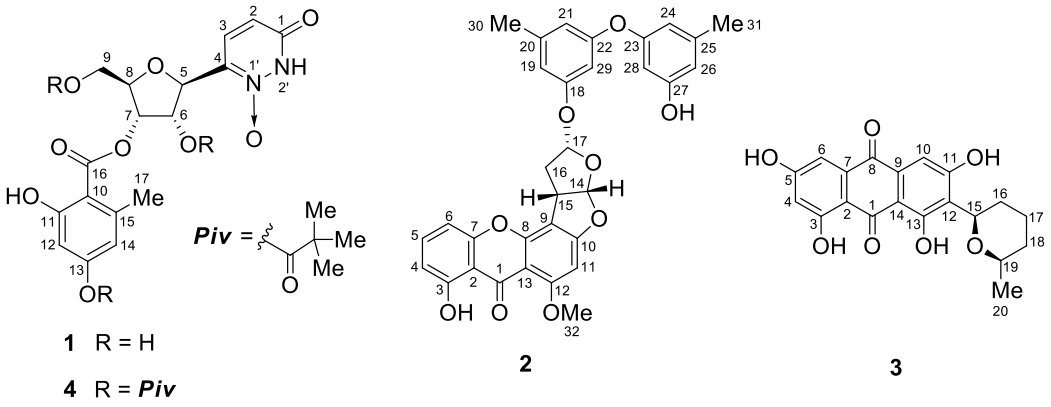

Figure 1. Structures of compounds **1**–**4.**

2. Results and discussion

Aspergilin A (**1**) was obtained as amorphous powder. The molecule formula $C_{17}H_{19}N_2O_9$ with ten degrees of unsaturation was determined by HR-ESIMS (*m*/*z*: calcd: 395.1085; found: 395.1084 [M + H]$^+$). The ^{13}C-NMR spectroscopic data and DEPT 135 experiment of **1** revealed the presence of a methyl group, an oxygenated methylene group, eight methine groups (four oxygenated and four olefinic), and seven quaternary carbons (two carbonyl and five olefinic). According to the 1D and 2D NMR spectroscopic data of **1**, nine degrees of unsaturation are due to a carbon–carbon double bond, a carbon–nitrogen double bond, a tetrahydrofuran ring, an amide group, and a benzoate group. Thus, a pyridazinone ring should be existed in the molecule.

The presence of a β-D-ribofuranose unit (**1a**), being characterized by the corresponding NMR spectroscopic data [δ_H 5.96 (d, J = 6.4 Hz, H-5), 4.46 (dd, J = 11.0, 5.8 Hz, H-6), 6.00 (d, J = 5.6 Hz, 6-OH), 5.45 (dd, J = 5.2, 2.8 Hz, H-7), 4.26 (dd, J = 5.4, 2.8 Hz, H-8), 3.74 (br s, H_2-9), 5.38 (t, J = 4.8 Hz, 9-OH); δ_C 87.8 (CH, C-5), 72.0 (CH, C-6), 74.0 (CH, C-7), 83.0 (CH, C-8), 61.2 (CH_2, C-9)] (Table 1), was corroborated by ^{1}H–^{1}H COSY correlations between H-5/H-6, H-6/H-7, H-7/H-8, and H-8/H_2-9 (Figure 2a). The existence of an orsellinic acid moiety (**1b**), i.e., a 2,4-dihydroxy-6-methylbenzoic acid unit, being evidenced by the corresponding NMR spectroscopic data [δ_H 6.24 (d, J = 2.0 Hz, H-12), 6.28 (d, J = 2.0 Hz, H-14), 2.47 (s, H_3-17), 10.85 (s, 11-OH), 10.17 (s, 13-OH); δ_C 106.3 (qC, C-10), 162.6 (qC, C-11), 100.9 (CH, C-12), 162.1 (qC, C-13), 111.2 (CH, C-14), 142.4 (qC, C-15), 169.1 (qC, C-16), 23.1 (CH_3, C-17)](Table 1), was confirmed by HMBC correlations between OH-11/C-10, OH-11/C-11, OH-11/C-12, OH-13/C-12, OH-13/C-13, OH-13/C-14, H_3-17/C-10, H_3-17/C-14, H_3-17/C-15, and H_3-17/C-16. Strong HMBC cross-peaks from protons of Me-17 (δ_H 2.47, s) to the quaternary C-15 (δ_C 142.4) placed it at C-15. Most notably, the key HMBC cross-peak from H-7 to the carbonyl C-16 connected the β-D-ribofuranose unit (**1a**) and the orsellinic acid moiety (**1b**) through the C-7–O–C-16 bond (Figure 2a).

Table 1. ^{1}H- and ^{13}C-NMR Data for **1** in DMSO-d_6 and its derivative **4** in $CDCl_3$ (δ in ppm and *J* in Hz).

Position	**1**[a]		**4**[b]	
	δ_H, multi. (*J*)	**δ_C, type**	δ_H, multi. (*J*)	δ_C, type
1		163.3, qC		162.1, qC

Preprints (www.preprints.org) | NOT PEER-REVIEWED | Posted: 26 October 2023 doi:10.20944/preprints202310.1727.v1

2	5.78 d (8.0)	102.6, CH	5.79 d (8.0)	103.4, CH
3	7.96 d (8.0)	140.7, CH	7.39 d (8.0)	139.4, CH
4		151.1, qC		149.7, qC
5	5.96 d (6.4)	87.8, CH	6.06 d (6.3)	87.8, CH
6	4.46 dd (11.0, 5.8)	72.0, CH	5.47 t (6.3)	72.6, CH
7	5.45 dd (5.2, 2.8)	74.0, CH	5.65 t (4.9)	72.0, CH
8	4.26 dd (5.4, 2.8)	83.0, CH	4.56 m	80.4, CH
9	3.74 2H, br s	61.2, CH_2	4.39 dd (12.6, 2.8) 4.47 dd (12.6, 3.5)	63.4, CH_2
10		106.3, qC		108.6, qC
11		162.6, qC		164.9, qC
12	6.24 d (2.0)	100.9, CH	6.53 br s	117.0, CH
13		162.1, qC		156.2, qC
14	6.28 d (2.0)	111.2, CH	6.62 br s	108.9, CH
15		142.4, qC		142.9, qC
16		169.1, qC		170.1, qC
17	2.47 s	23.1, CH_3	2.66 s	24.6, CH_3
2'	11.40 s		8.19 s	
18				176.2, qC
19				38.9, qC
20			1.35 s	27.0, CH_3
21			1.35 s	27.0, CH_3
22			1.35 s	27.0, CH_3
23				177.9, qC
24				39.3, qC
25			1.27 s	27.3, CH_3
26			1.27 s	27.3, CH_3
27			1.27 s	27.3, CH_3
28				177.3, qC
29				38.8, qC
30			1.09 s	26.8, CH_3
31			1.09 s	26.8, CH_3
32			1.09 s	26.8, CH_3
6-OH	6.00 d (5.6)			
9-OH	5.38 t (4.8)			
11-OH	10.85 s		11.08 s	
13-OH	10.17 s			

[a] ^{1}H- and ^{13}C-NMR data measured at 400 and 100 MHz, respectively; [b] ^{1}H- and ^{13}C-NMR data measured at 700 and 175 MHz, respectively.

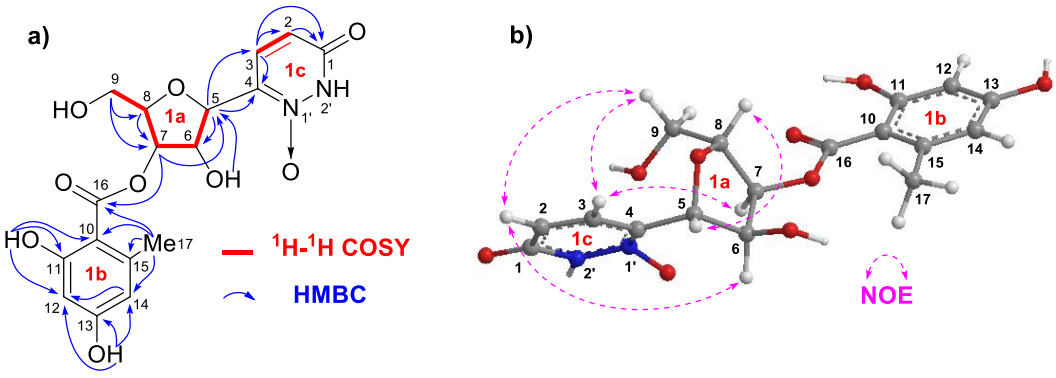

Figure 2. **a)** Selected ^{1}H–^{1}H COSY and HMBC correlations for **1**. **b)** Diagnostic NOE interactions for **1**.

Preprints (www.preprints.org) | NOT PEER-REVIEWED | Posted: 26 October 2023 doi:10.20944/preprints202310.1727.v1

The presence of a pyridazinone ring (**1c**), being characterized by the corresponding NMR spectroscopic data [δ_H 11.40 (s, H-2'), 5.78 (d, *J* = 8.0 Hz, H-2), 7.96 (d, *J* = 8.0 Hz, H-3); δ_C 163.3 (qC, C-1), 102.6 (CH, C-2), 140.7 (CH, C-3), 151.1 (qC, C-4)] (Table 1), was corroborated by the ^{1}H–^{1}H COSY cross-peak between H-2/H-3 and HMBC correlations between H-2/C-1, H-3/C-1, H-3/C-2, and H-3/C-4 (Figure 2a). The Key HMBC correlation from H-5 to C-4 connected the β-D-ribofuranose unit (**1a**) and the above pyridazinone ring (**1c**) through the C-4–C-5 bond. In addition, the existence of a nitrogen–oxygen bond could be inferred by the molecule formula of **1** to be loaded on $N_{1'}$. Taken together, the planar structure of **1** was elucidated as shown (Figure 2a).

The relative configuration of **1** was determined by NOE interactions (Figure 2b). Those between H-2/H-6, H-2/H_2-9, H_2-9/H-3, and H-3/H-7 revealed their cofacial relationship and were arbitrarily assigned as the α-oriented H-6 and H-7, whereas the diagnostic NOE interaction between H-5 and H-8 assigned their cofacial β-orientation. In order to reconfirm the constitution of **1** and establish its absolute configuration, single-crystal X-ray diffraction analysis was taken into account. However, it is impossible to get suitable crystals of **1** due to its poor solubility. Thus, derivatization reaction products were considered. Suitable crystals of **4** (a tri-pivaloyl derivative of **1**, Figure 1) were obtained after considerable effort. Finally, the constitution and absolute configuration of **1**, named aspergillin A, were established by single-crystal X-ray diffraction analysis of **4**, conducted with Cu Kα radiation [Flack parameter –0.12(9)] (Figure 3, CCDC 2291154). The absolute configuration of **1**, named aspergillin A, was unambiguously determined to be (5S,6S,7S,8R). To the best of our knowledge, aspergillin A is the first reported orsellinic acid–ribose–pyridazinone-N-oxide hybrid.

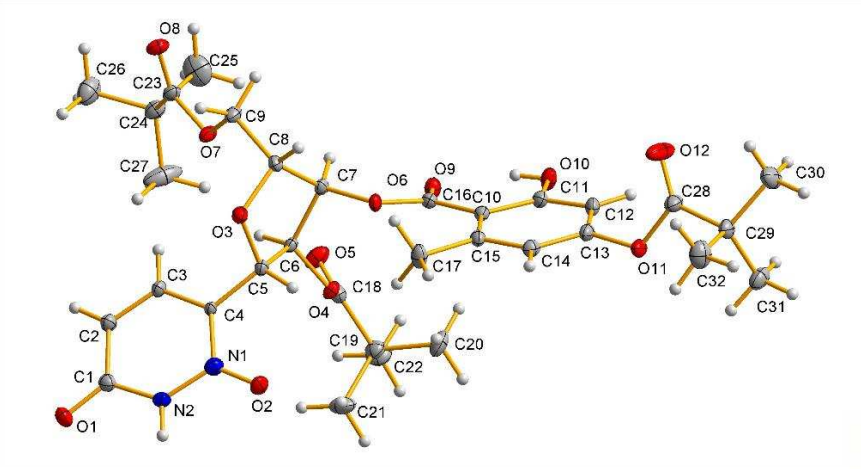

Figure 3. Oak Ridge Thermal-Ellipsoid Plot Program (ORTEP) illustration of the X-ray structure of **4** (Ellipsoids are given at the 30% probability level, Cu Kα).

Aspergilin B (**2**) was isolated as light white amorphous powder. The molecular formula $C_{32}H_{26}O_9$ was determined by the positive HR-ESIMS ion at *m/z* 555.1644 (calcd for $[M + H]^+$, 555.1650), indicating twenty degrees of unsaturation. According to ^{1}H- and ^{13}C-NMR spectroscopic data of **2** (Table 2), thirteen degrees of unsaturation are due to a keto-carbonyl function and twelve carbon–carbon double bonds. Therefore, the molecule has to be heptacyclic. The ^{13}C-NMR spectroscopic data and DEPT 135 experiment of **2** revealed the presence of three methyl groups (a methoxy and two tertiary), a methylene group, thirteen methine groups (twelve olefinic and one oxygenated), and fifteen quaternary carbons (one carbonyl, five olefinic, and nine oxygenated).

The NMR spectroscopic data of **2** resembled those of dihydrosterigmatocystin [26, 27], except for the presence of an additional 5,5'-oxybis(3-methylphenol) moiety, namely diorcinol [28, 29], being characterized by the corresponding NMR spectroscopic data [δ_H 6.67 (br s, H-19), 6.51 (br s, H-21), 6.400 (d, *J* = 2.0 Hz, H-24), 6.399 (d, *J* = 2.0 Hz, H-26), 6.29 (t, *J* = 2.0 Hz, H-28), 6.56 (d, *J* = 2.0 Hz, H-29), 2.30 (s, H_3-30), 2.27 (s, H_3-31), 4.71 (br s, 27-OH); δ_C 157.6 (qC, C-18), 112.0 (CH, C-19), 140.9 (qC, C-20), 114.0 (CH, C-21), 157.8 (qC, C-22), 158.2 (qC, C-23), 111.4 (CH, C-24), 141.0 (qC, C-25), 111.1 (CH, C-26), 156.5 (qC, C-27), 103.3 (CH, C-28), 105.1 (CH, C-29), 21.5 (Me-30), 21.7 (Me-31)]. The

Preprints (www.preprints.org) | NOT PEER-REVIEWED | Posted: 26 October 2023 doi:10.20944/preprints202310.1727.v1

existence of the diorcinol moiety was corroborated by HMBC correlations between H-19/C-18, H-19/C-21, H-19/C-29, H_3-30/C-19, H_3-30/C-20, H_3-30/C-21, H-21/C-22, H-24/C-23, H-24/C-28, H_3-31/C-24, H_3-31/C-25, H_3-31/C-26, 27-OH/C-26, 27-OH/C-27, and 27-OH/C-28. HMBC cross-peaks from protons of Me-30 (δ_H 2.30, s) to the quaternary C-20 (δ_C 140.9) and those from protons of Me-31 (δ_H 2.27, s) to the quaternary C-25 (δ_C 141.0) placed Me-30 at C-20 and Me-31 at C-25, respectively. In addition, the key HMBC correlation from H-17 (δ_H 5.89, t, J = 4.9 Hz) to the quaternary C-18 (δ_C 157.6, qC) connected the dihydrosterigmatocystin unit and the diorcinol moiety through the C-17–*O*–C-18 bond. Therefore, the constitution of **2** was elucidated as shown (Figure 4).

Table 2. ^{1}H- and ^{13}C-NMR Data for **2** and dihydrosterigmatocystin (δ in ppm and J in Hz).

Positon	**2 ($CDCl_3$)[a]**		dihydrosterigmatocystin (DMSO-d_6) [26]	
	δ_H, multi. (J)	**δ_C, type**	δ_H, multi. (J)	δ_C, type
1		181.4, qC		180.0, qC
2		109.0, qC		108.1, qC
3		162.3, qC		161.3, qC
4	6.77 d (8.0)	111.4, CH	6.73 dd (8.5, 1.0)	110.5, CH
5	7.52 t (8.0)	135.8, CH	7.61 t (8.5)	136.0, CH
6	6.83 d (8.0)	105.9, CH	6.94 dd (8.5, 1.0)	106.1, CH
7		154.9, qC		154.4, qC
8		154.5, qC		153.8, qC
9		106.6, qC		105.4, qC
10		164.8, qC		165.8, qC
11	6.43 s	90.6, CH	6.60 s	90.2, CH
12		163.7, qC		162.9, qC
13		106.1, qC		104.8, qC
14	6.56 d (5.6)	112.3, CH	6.55 d (5.5)	113.4, CH
15	4.37 m	42.5, CH	4.25 m	43.3, CH
16	2.61 m, 2.73 m	37.4, CH_2	2.24 m, 2.45 m	30.7, CH_2
17	5.89 t (4.9)	103.3, CH	3.54 m, 4.10 m	67.2, CH_2
18		157.6, qC		56.5, OCH_3
19	6.67 br s	112.0, CH		
20		140.9, qC		
21	6.51 br s	114.0, CH		
22		157.8, qC		
23		158.2, qC		
24	6.400 d (2.0)	111.4, CH		
25		141.0, qC		
26	6.399 d (2.0)	111.1, CH		
27		156.5, qC		
28	6.29 t (2.0)	103.3, CH		
29	6.56 d (2.0)	105.1, CH		
30	2.30 s	21.5, CH_3		
31	2.27 s	21.7, CH_3		
32	4.01 s	56.9, CH_3		
3-OH	13.22 s		13.38 s	
27-OH	4.71 br s			

[a] ^{1}H and ^{13}C NMR data measured at 700 and 175 MHz, respectively.

Preprints (www.preprints.org) | NOT PEER-REVIEWED | Posted: 26 October 2023 doi:10.20944/preprints202310.1727.v1

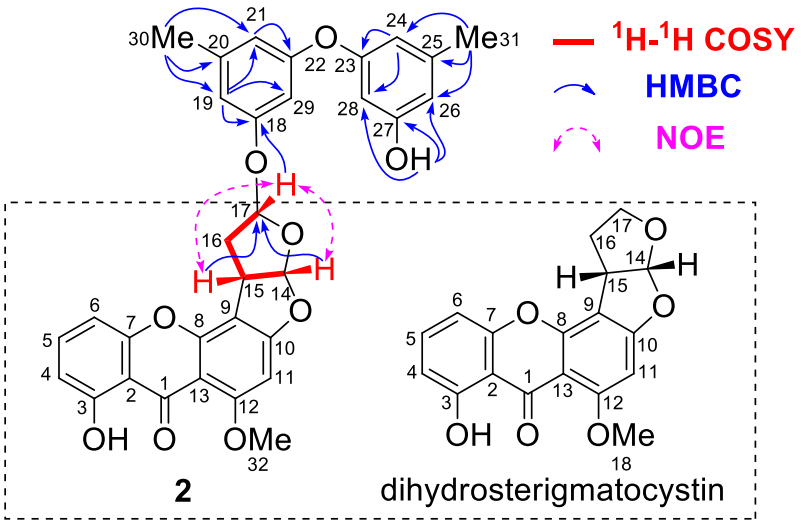

Figure 4. Selected ^{1}H–^{1}H COSY cross-peaks, HMBC correlations, and NOE interactions for **2**.

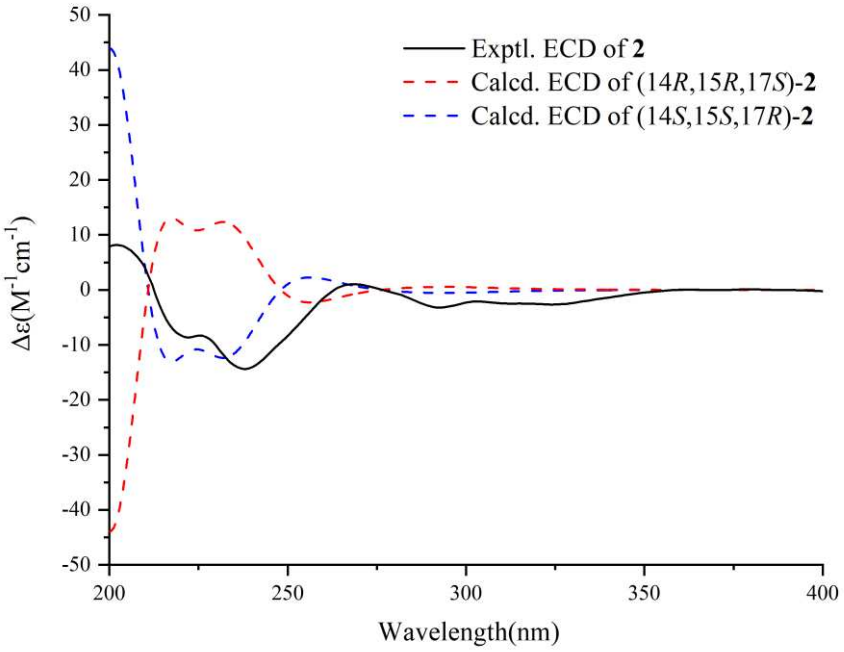

Figure 5. Experimental and calculated ECD curves for **2**.

The relative configuration of **2** was determined by NOE interactions (Figure 4). Those between H-17/H-14 and H-17/H-15 revealed their cofacial relationship. Based on the previous reported absolute configuration of dihydrosterigmatocystin, the absolute configuration of C-17 in **2** was thereby assigned as *R*. In addition, the absolute configuration of **2** was reconfirmed by quantum-chemical electronic circular dichroism (ECD) calculations. The calculated ECD curve of (14*S*,15*S*,17*R*)-**2** showed good agreement with that of the experimental curve of **2** (Figure 5), whereas that of (14*R*,15*R*,17*S*)-**2** exhibited mirrored Cotton effects. Therefore, the absolute configuration of **2**, named aspergilin B, was concluded to be (14*S*,15*S*,17*R*).

Compound **3** was obtained as amorphous powder. The molecular formula $C_{20}H_{18}O_7$ was established by the positive HR-ESIMS ion at m/z 371.1136 (calcd for $[M + H]^+$, 371.1125), indicating twelve degrees of unsaturation. According to the NMR spectroscopic data of **3** (Table 3), eight degrees of unsaturation are due to two keto-carbonyl function, six carbon–carbon double bonds. Therefore,

Preprints (www.preprints.org) | NOT PEER-REVIEWED | Posted: 26 October 2023 doi:10.20944/preprints202310.1727.v1

the molecule has to be tetracyclic. The presence of a 3,5,11,13-tetrahydroxyanthraquinone core, being characterized by the corresponding NMR spectroscopic data [δ_H 6.51 (d, J =1.2 Hz, H-4), 7.03 (br s, H-6), 7.00 (s, H-10); δ_C 188.5 (qC, C-1), 108.4 (qC, C-2), 165.5 (qC, C-3), 108.0 (CH, C-4), 164.3 (qC, C-5), 109.0 (CH, C-6), 134.7 (qC, C-7), 181.0 (qC, C-8), 133.1 (qC, C-9), 109.0 (CH, C-10), 161.5 (qC, C-11), 119.8 (qC, C-12), 162.9 (qC, C-13), 108.2 (qC, C-14)], was confirmed by HMBC correlations between H-4/C-2, H-4/C-5, H-10/C-1, H-10/C-8, H-10/C-12, and H-10/C-14. The presence of a 20-methyltetrahydropyran moiety was confirmed by ^{1}H–^{1}H COSY cross-peaks between H-15/H$_2$-16, H$_2$-16/H$_2$-17, H$_2$-17/H$_2$-18, H$_2$-18/H-19, and H-19/H$_3$-20 and HMBC correlations between H-15/C-11, H-15/C-12, H-15/C-13, H-15/C-16, H-15/C-19, H$_3$-20/C-18, H$_3$-20/C-19. HMBC correlations from H-15 to C-11, C-12, and C-13 connected the 3,5,11,13-tetrahydroxyanthraquinone core and the 20-methyltetrahydropyran moiety through the C-12–C-15 bond (Figure 6a).

Table 3. ^{1}H- and ^{13}C-NMR Data for **3** in DMSO-d$_6$ (δ in ppm and J in Hz).

Positon	**3**[a]	
	δ_H, multi. (J)	δ_C, type
1		188.5, qC
2		108.4, qC
3		165.5, qC
4	6.51 d (1.2)	108.0, CH
5		164.3, qC
6	7.03 br s	109.0, CH
7		134.7, qC
8		181.0, qC
9		133.1, qC
10	7.00 s	109.0, CH
11		161.5, qC
12		119.8, qC
13		162.9, qC
14		108.2, qC
15	4.94 d (10.8)	73.3, CH
16	1.60 m, 1.93 m	28.3, CH$_2$
17	1.63 m, 1.87 m	23.4, CH$_2$
18	1.30 m, 1.65 m	32.5, CH$_2$
19	3.61 m	74.6, CH
20	1.18 d (6.0)	21.9, CH$_3$

[a] ^{1}H and ^{13}C NMR data measured at 400 and 100 MHz, respectively.

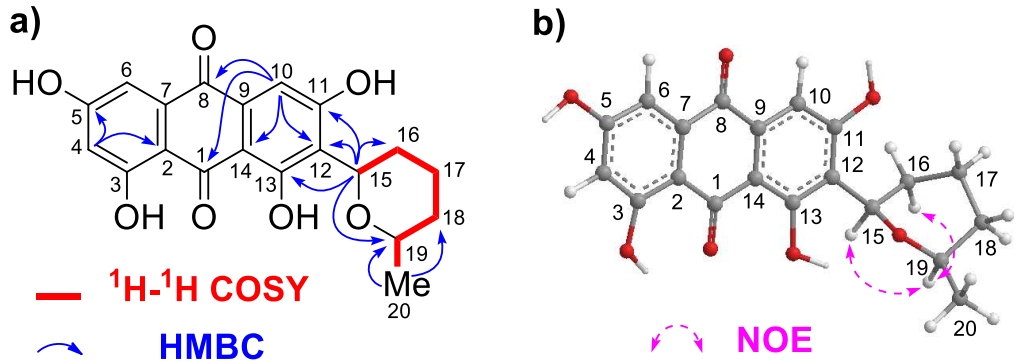

Figure 6. a) Selected ^{1}H–^{1}H COSY and HMBC correlations for **3**. **b)** Diagnostic NOE interactions for **3**.

Preprints (www.preprints.org) | NOT PEER-REVIEWED | Posted: 26 October 2023 doi:10.20944/preprints202310.1727.v1

The strong NOE interaction between H-15 and H-19 revealed their cofacial relationship (Figure 6b). The NMR spectroscopic data of **3** were the same as those of averufanin [21, 22, 25]. However, two absolute configurations, viz., (15*R*,19*R*) and (15*S*,19*S*), were confused in literatures [20–25]. In order to clarify the absolute configuration of **3**, quantum-chemical ECD calculations were employed. The calculated ECD curve of (15*R*,19*R*)-**3** showed good agreement with that of the experimental curve of **3**, whereas that of (15*S*,19*S*)-**3** exhibited mirrored Cotton effects (Figure 7). Therefore, the absolute configuration of **3**, i.e., averufanin, was concluded to be (15*R*,19*R*).

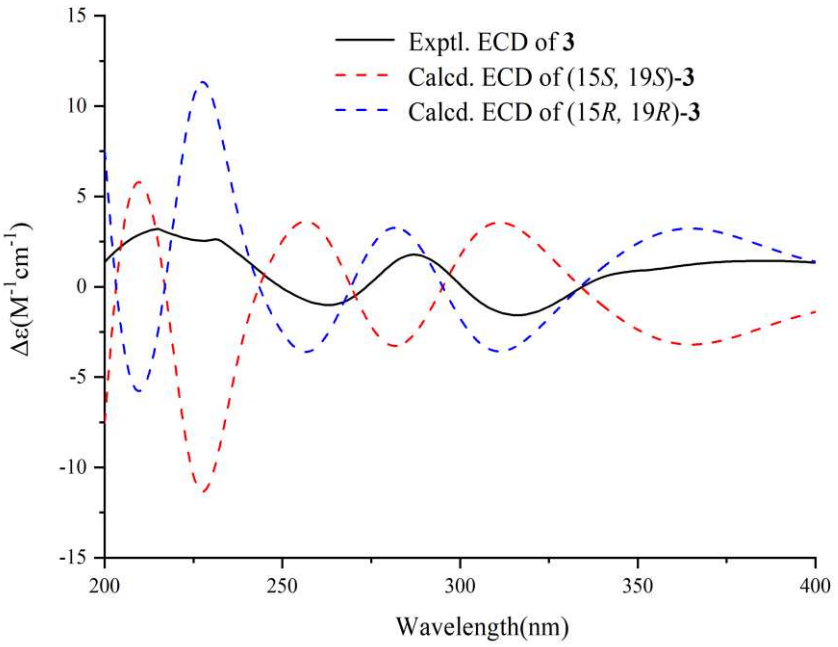

Figure 7. Experimental and calculated ECD curves for **3**.

The biosynthetic origin of **1** could be traced back to three building blocks, viz., 3-oxo-2,3-dihydropyridazine 1-oxide, β-D-ribofuranose, and orsellinic acid, among which the 3-oxo-2,3-dihydropyridazine 1-oxide moiety could be originated from one unit of *L*-glutamic acid, whereas the orsellinic acid unit could be biosynthesized from four units of acetyl coenzyme A (Scheme 1). The amidation of *L*-glutamic acid could generate *L*-glutamine, of which the decarboxylation and dehydrogenation would produce the intermediate (*E*)-4-aminobut-2-enamide. Subsequent cyclization and dehydrogenation could afford the heterocyclic intermediate pyridazin-3(2*H*)-one, of which the oxidation at the nitrogen atom would yield the crucial building block 3-oxo-2,3-dihydropyridazine 1-oxide. Finally, the generation of a new carbon–carbon bond between C-6 of the 3-oxo-2,3-dihydropyridazine 1-oxide moiety and C-1 of the β-D-ribofuranose motif, along with dehydration, followed by the esterification between 3-OH of the β-D-ribofuranose motif and the 7-carboxyl group of the orsellinic acid unit could give aspergilin A (**1**). (Scheme 1)

Preprints (www.preprints.org) | NOT PEER-REVIEWED | Posted: 26 October 2023 doi:10.20944/preprints202310.1727.v1

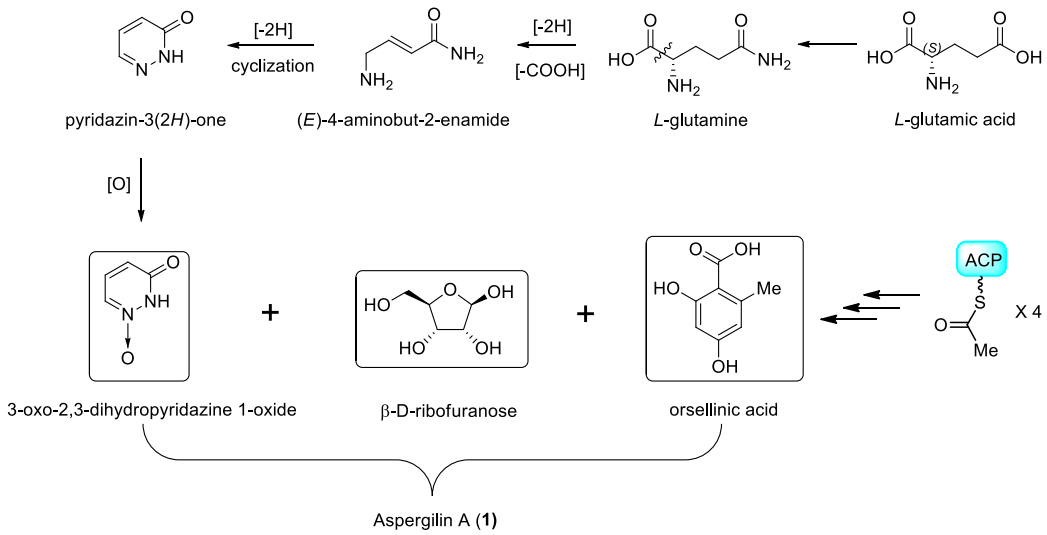

Scheme 1. Proposed biosynthetic origin of aspergilin A (**1**).

The antiproliferative activity of compounds **1**–**3** against four cancer cell lines were evaluated by using the standard MTT assay, with MS-275 (a known anticancer agent) as the positive control. As summarized in Table 4 and Figure 8, compound **2** is the most potent one among the three compounds with IC_{50} values of 8.83, 14.18, and 15.12 μM against HepG2, LLC, and B16-F10 cancer cell lines, respectively. Compounds **1** and **3** showed lower activities with IC_{50} values around or greater than 50.0 μM.

Table 4. *In vitro* antiproliferative activities of **1**–**3**.

Compounds	IC_{50} (μM) ± SD			
	HepG2	**LLC**	B16-F10	MCF7
1	> 50.0	> 50.0	> 50.0	> 50.0
2	8.83 ± 3.43	14.18 ± 3.84	15.12 ± 1.45	> 50.0
3	39.86 ± 1.27	> 50.0	48.63 ± 1.20	> 50.0
MS-275[a]	1.01 ± 0.25	5.36 ± 1.05	4.00 ± 0.28	14.74 ± 0.44

[a] MS-275 was used as a positive control.

Preprints (www.preprints.org) | NOT PEER-REVIEWED | Posted: 26 October 2023 doi:10.20944/preprints202310.1727.v1

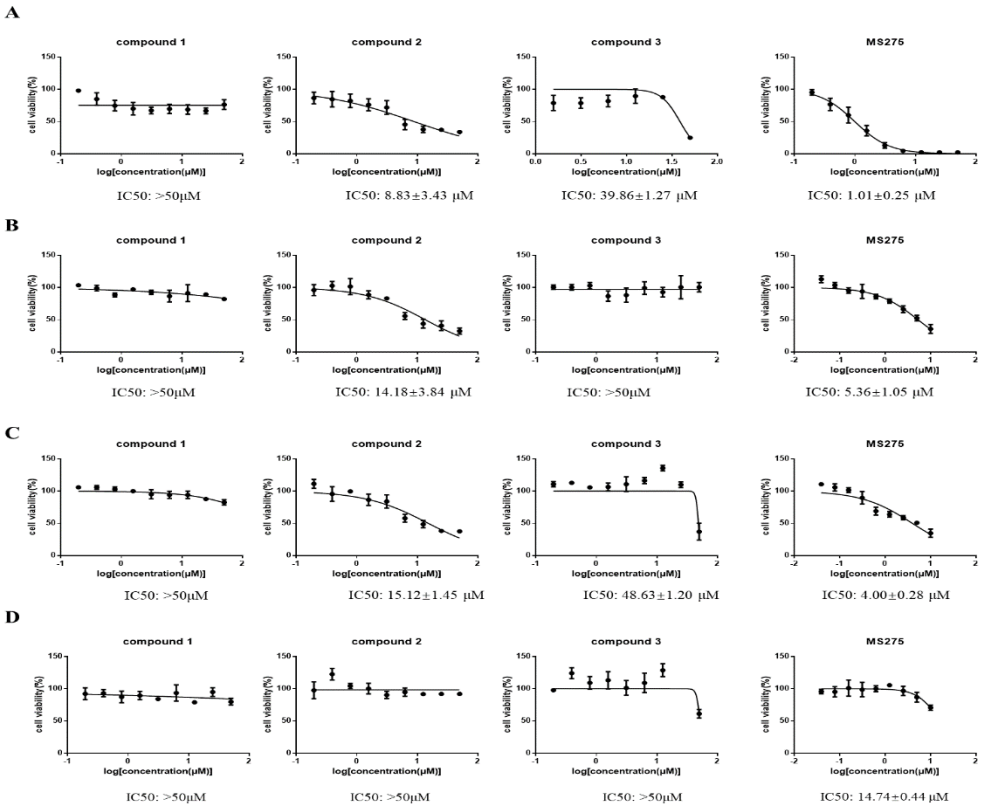

Figure 8. (A) MTT curve graph of compounds **1**–**3** and MS-275 against HepG2 cells. (B) MTT curve graph of compounds **1**–**3** and MS-275 against LLC cells. (C) MTT curve graph of compounds **1**–**3** and MS-275 against B16-F10 cells. (D) MTT curve graph of compounds **1**–**3** and MS-275 against MCF7 cells.

The most potent compound **2** was selected to evaluate its effects on the cell cycle of HepG2 cancer cells using flow cytometry. As shown in **Figure 9A/B,** after treatment with increasing concentrations of compound **2** (4.0, 8.0, and 16.0 μM) for 48h, the percentages of cells arrested at G2/M phase were increased from 14.83 % to 25.91 %, as compare to the control group (15.03%). Therefore, compound **2** could dose-dependently induce G2/M phase arrest in HepG2 cells.

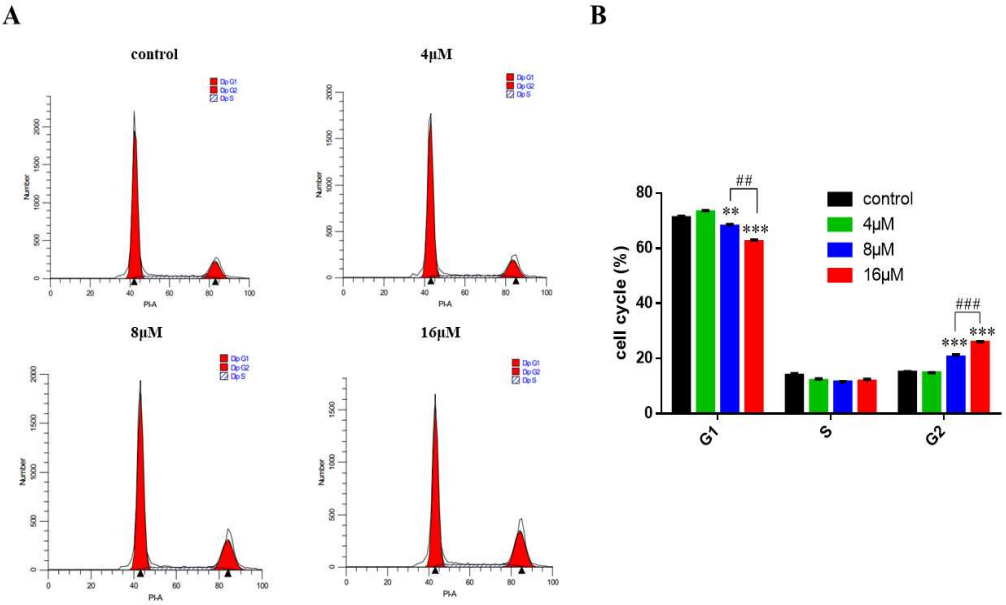

 doi:10.20944/preprints202310.1727.v1

Figure 9. Cell cycle arrest induced by compound **2**. (A) HepG2 cells were incubated with varying concentrations of compound **2** (4.0, 8.0, and 16.0 μM) for 48 h. (B) Histograms showing the percentage of cell cycle distribution following compound **2** treatment (n = 3). The bar graphs are presented as mean ± SD. ***P < 0.001, ** P < 0.01, * P < 0.05 compared with the corresponding control group, ###P < 0.001, ##P <0.01 compared with the 16.0 μM-treated group, One-way ANOVA.

3. Materials and Methods

3.1. General experimental procedures

HR-ESIMS spectra were obtained on a Bruker Daltonics Apex-Ultra 7.0 T (Bruker Corporation, Billerica, MA, USA). Optical rotations were recorded on an MCP500 modular circular polarimeter (Anton Paar GmbH) with a 0.5 cm cell at 25 °C and UV spectra measured on a UV-2600 UV-Vis spectrophotometer (SHIMADZU) at room temperature. IR spectra were obtained on a SHIMADZU IRAffinity-1 Fourier transform infrared spectrometer and ECD spectra recorded on a circular dichromatic spectrometer (Chirascan, Applied PhotoPhysics, UK). X-ray data were collected using an Agilent SuperNova with AtlasS2 X-ray single-crystal diffractometer with Cu Kα radiation. 1D and 2D NMR spectra were measured on a Bruker AV-400 or 700 MHz NMR spectrometer. High performance liquid chromatography (HPLC) was performed on a Waters 2535 pump equipped with a 2998 photodiode array detector and C_{18} reversed-phase columns (YMC, Kyoto, Japan; 250 mm × 4.6 mm, length × i.d., 5 μm, for analysis; 250 mm × 10 mm, length × i.d., 5 μm, for preparation). Silica gel (QingDao Hai Yang Chemical Group Co.; 100–200 and 200–300 mesh) and octadecylsilyl silica gel (YMC, Japan, ODS-A-HG12nm, 50 μm) were used for column chromatography (CC).

3.2. Fungus material

The fungal strain *Aspergillus* sp. A1E3 was isolated from the fruit of *Rhizophora mucronata*, collected from the Thai mangrove swamps of the Trang Province in February 2012. It was identified as *Aspergillus* sp. according to ITS rDNA sequence data. The strain was preserved in School of Pharmaceutical Sciences, Southern Medical University.

3.3. Fermentation, Extraction and isolation

The Fungal strain *Aspergillus* sp. A1E3 was inoculated into Erlenmeyer flasks (500 mL) containing 10‰ sea salt and potato glucose solution in a sterile environment at 25 °C for seven days to prepare the seed culture, which was then inoculated into 100 Erlenmeyer flasks (1000 mL) each containing rice solid medium (100 g rice and 150 mL water containing 10‰ sea salt) at room temperature in static conditions for 28 days. Then the fermentation material of *Aspergillus* sp. A1E3 was extracted three times with EtOAc, which was evaporated under vacuum. The resulting EtOAc extract was dissolved in EtOAc again and washed three times with water. The EtOAc solution was dried under reduced pressure and then dissolved in MeOH. After washing with *n*-hexane for three times, the remaining MeOH solution was dried to yield the resulting solid extract (70.11g), which was then fractionated by a silica gel column chromatography (200-300 mesh silica, 180 × 10 cm, id) with a gradient mixture of $CHCl_3$/MeOH (v/v, 100:0, 100:1, 50:1, 98:2, 30:1, 20:1, 10:1, 5:1, 3:1, 2:1, 1:1, 1:2) to afford 170 fractions. Fr. 42 and Fr.43 were combined (3.89 g) and subjected to a C_{18} reversed-phase column (60 × 6 cm, i.d.), eluted with a gradient mixture of acetone/H_2O (v/v, 50:50 to 100:0) to afford 70 subfractions. Then subfractions 22 and 23 were combined and further purified by semi-preparative HPLC (MeCN:H_2O 58:42) to yield **2** (1.0 mg, t_R = 90.0 min). Fr. 44 (1.01 g) was subjected to a C_{18} reversed-phase column (60 × 6 cm, i.d.), eluted with a gradient mixture of acetone/H_2O (v/v, 50:50 to 100:0) to give 50 subfractions, among which subfraction 46 (112.6 mg) was further purified by semi-preparative HPLC (CH_3CN:H_2O 65:35) to afford **3** (40.0 mg, t_R = 68.8min). Fr. 145 (238.0 mg) was dissolved in chloroform and then filtered to give **1** (50.0 mg).

3.4. Spectroscopic data of compounds

Aspergilin A (**1**): White amorphous powder; $[\alpha]_D^{25}$ – 25.4 (*c* 0.10, MeOH); UV (MeOH) λ_{max} (logε) 213 (1.81) nm; IRυ_{max} 3744, 3649, 3443, 3256, 2361, 2338, 1713, 1678, 1616, 1443, 1379, 1323, 1252, 1173,

 doi:10.20944/preprints202310.1727.v1

1136, 1065 cm^{-1}; ^{1}H and ^{13}C NMR spectroscopic data, see Table 1; HR-ESIMS *m/z* 395.1084 $[M + H]^+$ (calcd for $C_{17}H_{20}N_2O_9$, 395.1085).

Aspergilin B (**2**): Light white amorphous powder; $[\alpha]_D^{25}$ – 57.6 (*c* 0.10, MeOH); UV (MeOH) λ_{max} (logε) 206 (1.52) nm; IRυ_{max} 3439, 2918, 2851, 2359, 1647, 1620, 1582, 1460, 1233, 1155, 1040 cm^{-1}; ^{1}H and ^{13}C NMR spectroscopic data, see Table 2; HR-ESIMS *m/z* 555.1644 $[M + H]^+$ (calcd for $C_{32}H_{27}O_9$, 555.1650).

Aspergilin C (**3**): Deepred amorphous powder; $[\alpha]_D^{25}$ + 27.8 (*c* 0.05, MeOH); UV (MeOH) λ_{max} (logε) 208 (1.88) nm; IRυ_{max} 3566, 3385, 3231, 2932, 2859, 2359, 2342, 1614, 1395, 1254, 1207, 1167, 1072, 1024, 995 cm^{-1}; ^{1}H and ^{13}C NMR spectroscopic data, see Table 3; HR-ESIMS *m/z* 371.1136 $[M + H]^+$ (calcd for $C_{20}H_{19}O_7$, 371.1125).

3.5. X-ray crystallographic data of 4

$C_{32}H_{42}N_2O_{12}$, Mr 646.67, Colorless crystal from MeOH (mp 184.6-185.5), Temperature/K: 149.99(10). Crystal system: orthorhombic, Space group: P21212, a = 10.90168(15) Å, b = 11.02307(18) Å, c = 28.1523(4) Å, α: 90°, β: 90°, γ: 90°, Volume: 3383.06(9) Å3, Z: 4, ϱcalcg: 1.270 cm^3, μ: 0.816 mm^{-1}, F(000): 1376.0, Crystal size: 0.26 × 0.05 × 0.03 mm^3, Radiation: CuKα (λ = 1.54184), 2^{Θ} range for data collection: 6.28 to 129.988°, Index ranges: -12 ≤ h ≤ 12, -12 ≤ k ≤ 9, -33 ≤ l ≤ 33, Reflections collected: 15534, Independent reflections 5739 [R_{int} = 0.0313, R_{sigma} = 0.0343], Data/restraints/parameters: 5739/35/426, Goodness-of-fit on F^2: 1.049, Final R indexes [I>=2σ (I)]: R_1 = 0.0415, wR_2 = 0.1143, Final R indexes [all data]: R_1 = 0.0439, wR_2 = 0.1172, Largest diff. peak/hole: 0.73/-0.61 e $Å^{-3}$, Flack parameter: -0.12(9) (CCDC 2291154).

3.6. Synthesis of the derivative 4

Compound **1** (20.0 mg) was dissolved in pyridine (0.5 mL). DMAP (3.0 mg) was then added, along with 50.0 μL pivaloyl chloride under ice bath and stirred for 10 min. After the completion of the reaction (monitored by thin-layer chromatography, i.e., TLC), the last reaction mixture was concentrated under reduced pressure. The resulting residue was dissolved in methanol and purified by semi-preparative HPLC, eluted with the mixture of MeCN/H_2O (v/v, 58 : 42, 3.0 mL/min) to afford **4** (5.0 mg). Suitable crystals of **4** were obtained in MeOH after considerable effort.

3.7. Cell culture and cytotoxicity (MTT) assay

MTT assay was used to determine the antiproliferative activities of compounds **1-3** and MS-275 (positive control) against four cancer cell lines including human lung cancer cell line (HepG2), mouse Lewis lung carcinoma (LLC) cells, mouse skin melanoma cell line (B16-F10), human breast cancer cell line (MCF-7). Fetal bovine serum (FBS, 10%) in RPMI-1640 medium was used to culture MCF-7 cell lines and Fetal bovine serum (FBS, 10%) in DMEM medium was used to culture B16-F10, HepG2 and LLC. Cells were seeded into 96-well plates at a density of 5000 cells/well, incubated at 37℃ with 5% CO_2 overnight. The next day, the three compounds and MS-275 (InvivoChem) were dissolved in complete medium to prepare different concentrations of solution which were added to each well, followed by incubation at 37 ℃ for 48 h. Finally, 20 μL MTT (5 mg/mL dissolved in PBS) was added to each well and incubated with cells at 37℃ for 4 h. Then, the complete medium was removed and the formazan crystals were dissolved in 100 μL DMSO each well. The absorbance was measured in a TECAN microplate reader at 490 nm. GraphPad Prism was utilized to calculate the IC50s by a model of nonlinear regression to fit normalized dose response. All of the experiments were performed independently three times.

3.8. Cell cycle analysis.

To a six-well plate were seeded HepG2 cells at a density of 5×10^5 cells/well followed by incubation at 37 ℃ for overnight. Then, different concentrations of compounds **1-3** (4, 8, 16 μM) were added to the plate and incubated for 48 h. The collected cells were washed once with PBS. Then, the cells were added 1 mL DNA staining solution and 10 μL Permeabilization solution followed by incubation in dark for 30 min. The DNA content of samples was analyzed by flow cytometry.

4. Conclusions

In summary, two new compounds, named aspergilins A and B, were obtained from the rice culture of the mangrove endophytic fungus *Aspergillus* sp. A1E3, together with the known compound averufanin. The structures and absolute configurations of these compounds were established by extensive NMR investigations, quantum-chemical ECD calculations, and single-crystal X-ray diffraction analysis. The absolute configuration of aspergillin A was unambiguously determined by single-crystal X-ray diffraction analysis of its *tri*-pivaloyl derivative, conducted with Cu Kα radiation, whereas that of averufanin was first clarified by ECD calculations. Aspergilin A is the first reported orsellinic acid–ribose–pyridazinone-*N*-oxide hybrid containing a unique β-oxo-2,3-dihydropyridazine 1-oxide moiety, whereas aspergilin B is the sterigmatocystin derivative containing an additional diorcinol motif. From the perspective of biosynthesis, aspergilin A could be originated from the combined assembly of three building blocks, viz., orsellinic acid, β-D-ribofuranose, and *L*-glutamine. It is an unprecedented alkaloid-*N*-oxide involving biosynthetic pathways of polyketide, pentose, and amino acid. Aspergilin B (**2**) exhibits potent antiproliferative activity against a panel of cancer cell lines. Additionally, Aspergilin B (**2**) could dose-dependently induce G2/M phase arrest in HepG2 cells. This work demonstrates that mangrove endophytic fungi of the genus *Aspergillus* harbor secondary metabolites with new structures.

Supplementary Materials: The following supporting information can be downloaded at: www.mdpi.com/xxx/s1, HR-ESIMS, 1D and 2D NMR spectra of compounds **1–4**, UV and IR spectra of compounds **1–3**, along with energy analyses of conformers for compounds **2** and **3**.

Author Contributions: B.W. carried out the chemistry work under the guidance of G.C., whereas C.X. performed the antitumor work under the guidance of J.C.; B.W. and C.X. prepared the first draft of the manuscript; G.C. and J.C. helped with all the methodological approaches and finalized the paper. All authors have read and agreed to the published version of the manuscript.

Funding: This research was funded by National Natural Science Foundation of China (22177023), Key Science and Technology Program of Hainan Province (ZDKJ202008), and Hainan Provincial Natural Science Foundation of China (221RC1054).

Institutional Review Board Statement: Not applicable.

Data Availability Statement: Raw data discussed in this study are available in Supplementary Materials.

Acknowledgments: The authors gratefully thank Dr. Patchara Pedpradab (Rajamangala University of Technology Srivijaya, Trang Province, Thailand) for providing mangrove fruits used in this work.

Conflicts of Interest: The authors declare no conflict of interest.

References

1. Chintakunta, V.K.; Akella, V.; Vedula, M.S.; Mamnoor, P.K.; Mishra, P.; Casturi, S. R.; Vangoori, A.; Rajagopalan, R. 3-*O*-Substituted benzyl pyridazinone derivatives as COX inhibitors. *Eur. J. Med. Chem.* **2002**, *37*, 339–347.
2. Coelho, A.; Sotelo, E.; Novoa, H.; Peeters, O.M.; Blaton, N.; Raviña, E. Pyridazine derivatives. Part 38: Efficient Heck alkenylation at position 5 of the 6-phenyl-3(2*H*)-pyridazinone system. *Tetrahedron Lett.* **2004**, *45*, 3459–3463.
3. Gong, Y.; Barbay, J.K.; Dyatkin, A.B.; Miskowski, T.A.; Kimball, E.S.; Prouty, S.M.; Fisher, M.C.; Santulli, R.J.; Schneider, C.R.; Wallace, N.H.; Ballentine, S.A.; Hageman, W.E.; Masucci, J.A.; Maryanoff, B.E.; Damiano, B.P.; Andrade-Gordon, P.; Hlasta, D.J.; Hornby, P.J.; He, W. Synthesis and biological evaluation of novel pyridazinone-based α_4 integrin receptor antagonists. *J. Med. Chem.* **2006**, *49*, 3402–3411.
4. Rathish, I.G.; Javed, K.; Bano, S.; Ahmad, S.; Alam, M.S.; Pillai, K.K. Synthesis and blood glucose lowering effect of novel pyridazinone substituted benzenesulfonylurea derivatives. *Eur. J. Med. Chem.* **2009**, *44*, 2673–2678.
5. Schoene, D.L.; Hoffmann, O.L. Maleic hydrazide, a unique growth regulant. *Science*, **1949**, *109*, 588–589.
6. Shipp, J. L.; Wang, K.; Ferguson, G. Residual toxicity of avermectin b1 and pyridaben to eight commercially produced beneficial arthropod species used for control of greenhouse pests. *Biol. Control* **2000**, *17*, 125–131.

7. Navarro, A.; Bández, M.J.; Gómez, C.; Repetto, M.G.; Boveris, A. Effects of rotenone and pyridaben on complex I electron transfer and on mitochondrial nitric oxide synthase functional activity. *J. Bioenerg. Biomembr.* **2010**, *42*, 405–412.
8. Sugimoto, N.; Osakabe, M. Cross-resistance between cyenopyrafen and pyridaben in the twospotted spidermite *Tetranychus urticae* (Acari: Tetranychidae). *Pest. Manag. Sci.* **2014**, *70*, 1090–1096.
9. Basistyi, V.S.; Frederich, J.H. Pyridazine *N*-oxides as photoactivatable surrogates for reactive oxygen species. *Org. Lett.* **2022**, *24*, 1907–1912.
10. Chen, S.H.; Cai, R.L.; Liu, Z.M.; Cui, H.; She, Z.G. Secondary metabolites from mangrove-associated fungi: source, chemistry and bioactivities. *Nat. Prod. Rep.* **2021**, *39*, 560–595.
11. Liu, X.; Fu, Y.; Zhou, Q.Q.; Wang, S.; Gao, L.; Lei, J.L.; Ke, A.B.; Li, Y.Y.; Zhang, X.X.; Huo, C.H.; Lu, X.H. Aspergichromones A–E, five chromone derivatives with complicated polycyclic architecture from *Aspergillus deflectus*. *Org. Lett.* **2022**, *24*, 1610–1615.
12. Liu, L.; Duan, F.F.; Gao, Y.; Peng, X.G.; Chang, J.L.; Chen, J.; Ruan, H.L. Aspersteroids A–C, Three Rearranged Ergostane-type Steroids from *Aspergillus ustus* NRRL 275. *Org. Lett.* **2021**, *23*, 9620–9624.
13. Wang, L.; Yang, J.; Huang, J.P.; Li, J.; Luo, J.Y.; Yan, Y.J.; Huang, S.X. Bisaspochalasins A–C: three cytochalasan homodimers with highly fused ring system from an endophytic *Aspergillus flavipes*. *Org. Lett.* 2020, *22*, 7930–7935.
14. Liu, L.; Wang, L.; Bao, L.; Ren, J.W.; Basnet, B.B.; Liu, R.X.; He, L.W.; Han, J.J.; Yin, W.B.; Liu, H.W. Versicoamides F–H, prenylated indole alkaloids from *Aspergillus tennesseensis*. *Org. Lett.* 2017, *19*, 942–945.
15. Kankanamge, S.; Khalil, Z.G.; Sritharan, T.; Capon, R.J. Noonindoles G–L: indole diterpene glycosides from the Australian marine-derived fungus *Aspergillus noonimiae* CMB-M0339. *J. Nat. Prod.* 2023, *86*, 508–516.
16. Neuhaus, G.F.; Loesgen, S. Antibacterial drimane sesquiterpenes from *Aspergillus ustus*. *J. Nat. Prod.* 2021, *84*, 37–45.
17. Guo, Y.J.; Ding, L.; Ghidinelli, S.; Gotfredsen, C.H.; Cruz, M. de la; Mackenzie, T.A.; Ramos, M.C.; Sánchez, P.; Vicente, F.; Genilloud, O.; Coriani, S.; Larsen, R.W.; Frisvad, J.C.; Larsen, T.O. Taxonomy driven discovery of polyketides from *Aspergillus californicus*. *J. Nat. Prod.* 2021, *84*, 979–985.
18. Wei, M.S.; Huang, L.P.; Li, Q.; Qiao, X.Y.; Zhao, Z.M.; Yin, J.; Fu, A.M.; Guo, J.R.; Hao, X.C.; Gu, L.H.; Wang, J.P.; Chen, C.M.; Zhu, H.C.; Zhang, Y.H. Spectasterols, aromatic ergosterols with 6/6/6/5/5, 6/6/6/6, and 6/6/6/5 ring systems from *Aspergillus spectabilis*. *J. Nat. Prod.* 2023, *86*, 1385–1391.
19. Yang, W.C.; Chen, T.; Tan, Q.; Zang, Z.M.; Chen, Y.; Ou, Y.H.; Li, G.; Hu, D.; Wang, B.; Yao, H.L.; She, Z.G. Plasmodium-resistant indole diterpenoid biosynthesis gene cluster derived from *Aspergillus oryzae* was activated by exogenous P450 gene *Ast B. J. Nat. Prod.* **2023**, *86*, 1392–1401.
20. Holkers, J.S.E.; Kagal, S.A.; Mulheirn, L.J.; White, P.M. Some new metabolites of *Aspergillus versicolor* and a revised structure for averufin. *Chem. Commun.* **1966**, *24*, 911–913.
21. Castonguay, A. Synthesis of (±)-averufanin, noraverufanin and bis-deoxyaverufanin. *Tetrahedron* **1979**, *35*, 1557–1563.
22. Sakai, K.; Ohte, S.; Ohshiro, T.; Matsuda, D.; Masuma, R.; Rudel, L.L.; Tomoda, H. Selective inhibition of Acyl-CoA: cholesterol acyltransferase 2 isozyme by flavasperone and sterigmatocystin from *Aspergillus* Species. *J. Antibiot.* **2008**, *61*, 568–572.
23. Shao, C.L.; Wang, C.Y.; Wei, M.Y.; Li, S.D.; She, Z.G.; Gu, Y.C.; Lin, Y.C. Structural and spectral assignments of six anthraquinone derivatives from the mangrove fungus (ZSUH-36). *Magn. Reson. Chem.* **2008**, *46*, 886–889.
24. Chen, M.; Shao, C.L.; Kong, C.J.; She, Z.G.; Wang, C.Y. A new anthraquinone derivative from a gorgonian-derived fungus *Aspergillus* sp.. *Chem. Nat. Compd.* **2014**, 50, 617-620.
25. Demirel1, D.; Ozkaya, F.C.; Ebrahim, W.; Sokullu, E.; Sahin, I.D. *Aspergillus Carneus* metabolite Averufanin induced cell cycle arrest and apoptotic cell death on cancer cell lines via inducing DNA damage. *Sci. Rep.* **2023**, *13*, 6460.
26. Zhu, F.; Lin, Y.C. Three xanthones from a marine-derived mangrove endophytic fungus. *Chem. Nat. Compd.* **2007**, *43*, 132–135.
27. Han, X.; Tang, X.L.; Luo, X.C.; Sun, C.X.; Liu, K.C.; Zhang, Y.; Li, P.L.; Li, G.Q. Isolation and identification of three new sterigmatocystin derivatives from the fungus *Aspergillus versicolor* guided by molecular networking approach. *Chem. Biodivers.* **2020**, *17*, e2000208.
28. Ebrahim, W.; El-Neketi, M.; Lewald, L.I.; Orfali, R.S.; Lin, W.; Rehberg, N.; Kalscheuer, R.; Daletos, G.; Proksch, P. Metabolites from the fungal endophyte Aspergillus austroafricanus in axenic culture and in fungal–bacterial mixed cultures. *J. Nat. Prod.* **2016**, *79*, 914–922.
29. Özkaya, F.C.; Ebrahim, W.; El-Neketi, M.; Tanrikul, T.T.; Kalscheuer, R.; Müller, W.E.G.; Guo, Z.Y.; Zou, K.; Liu, Z.; Proksch, P. Induction of new metabolites from sponge-associated fungus *Aspergillus carneus* by OSMAC approach. *Fitoterapia* **2018**, *131*, 9–14.

 doi:10.20944/preprints202310.1727.v1

disclaim responsibility for any injury to people or property resulting from any ideas, methods, instructions or products referred to in the content.